Received: 5 February 2024 | Revised: 5 July 2024 | Accepted: 19 August 2024

DOI: 10.1002/joc.8609

RESEARCH ARTICLE

International Journal of Climatology RMetS

Assessing South Indian Ocean tropical cyclone characteristics in HighResMIP simulations

Pardeep Pall[1] | **Alexandre S. Gagnon**[1] | **Massimo A. Bollasina**[2] | **Colin M. Zarzycki**[3] | **Yuner Huang**[4] | **Christopher T. S. Beckett**[4] | **Harinaivo Ramanantoanina**[5] | **Thomas P. S. Reynolds**[4]

[1]School of Biological and Environmental Sciences, Liverpool John Moores University, Liverpool, UK

[2]School of GeoSciences, University of Edinburgh, Edinburgh, UK

[3]Department of Meteorology and Atmospheric Science, Penn State University, University Park, Pennsylvania, USA

[4]School of Engineering, University of Edinburgh, Edinburgh, UK

[5]Université Magis, Antananarivo, Madagascar

Correspondence
Pardeep Pall, School of Biological and Environmental Sciences, Liverpool John Moores University, James Parsons Building, Byrom Street, Liverpool L3 3AF, UK.
Email: p.pall@ljmu.ac.uk

Funding information
Royal Society, Grant/Award Number: CHL\R1\180180

Abstract

Several damaging tropical cyclones (TCs) have occurred recently over the South Indian Ocean (SIO) region, causing enormous social and economic losses. Yet, while many studies have examined SIO TC characteristics using observations and reanalysis, only a few have assessed these characteristics specifically for this region in climate models, and fewer have investigated their projections under climate change. Here we do this for a historical (1980–2010) and future (2020–2050) period, using multimodel simulations from the High Resolution Model Intercomparison Project, as well as examine biases in the historical period relative to a reanalysis (ERA5). The models have horizontal resolutions of 25–50 km, which has enabled an improved ability to represent tropical cyclones globally in previous studies. TempestExtremes software is employed to detect tropical storm and cyclone tracks. In cases where TempestExtremes cannot be applied due to a lack of requisite variables in a dataset, we instead examine extreme wind speeds in that dataset. For the historical period, we find considerable variation in model biases compared to ERA5, which itself exhibits realistic spatial patterns of tracks and their monthly distribution. Models do at least agree on positive biases in track frequency east of Madagascar and somewhat in the Mozambique Channel. However, the models and ERA5 only produce Category 3 tropical cyclones at best. Wind speeds for 25 km resolution models have much larger positive biases than for 50 km ones, suggesting the former can simulate even higher-category tropical cyclones. Considerable intermodel variation is also found in track changes between the future and historical periods. No systematic intercategory pattern of change exists, and low signal-to-noise may obscure any such patterns in the limited timespan of available data. Thus, no meaningful conclusions can be drawn regarding changes in track intensity. Nevertheless, track frequency broadly decreases across models for the region, as does accumulated cyclone energy. An east-to-west shift in track location from east of Madagascar toward the

Mozambique Channel is also implied by track frequency and wind speed changes. Our findings provide information to potentially improve storm resiliency in this vulnerable region.

KEYWORDS
ERA5, HighResMIP, South Indian Ocean, tropical cyclones

1 | INTRODUCTION

Studies assessing the characteristics of tropical cyclones (TCs) over the South Indian Ocean (SIO) region in climate models are relatively few (e.g., Cattiaux et al., 2020; Malherbe et al., 2013; Muthige et al., 2018; Thompson et al., 2021; Vitart et al., 2003) compared to studies based on observations or reanalysis (e.g., Ash & Matyas, 2012; Bessafi & Wheeler, 2006; Bié & de Camargo, 2023, and references therein; Chang-Seng & Jury, 2010; Fitchett, 2018; Ho et al., 2006; Ibebuchi, 2022; Jury, 1993; Kuleshov et al., 2010; Leroux et al., 2018; Matyas, 2015; Mavume et al., 2009). SIO TC studies can also feature less prominently in global climate change assessments compared to other regions (e.g., Seneviratne et al., 2021). This may be partly due to a lack of high-quality, consistent observational-based data, which hinders long-term climate analysis (Bié & de Camargo, 2023; Fitchett, 2018; Kuleshov et al., 2010; Matyas, 2015; Mavume et al., 2009) and also due to limited modelling efforts (Tulet et al., 2021).

Devastating TCs nevertheless occur in the SIO region, extending roughly from the equator to below South Africa and from western Australia to eastern Africa (e.g., Knapp et al., 2010). In 2023, for example, TC Freddy formed northwest of Australia and traversed the entire Indian Ocean before making multiple landfalls in southeast Africa—making it the most prolonged and energetic TC on record globally and resulting in severe floods and fatalities (JBA Risk Management, 2023). Other recent TCs causing severe devastation and several hundred million US dollars of damage include Batsirai in 2022 (AON, 2022), Kenneth and Idai in 2019 (Nhundu et al., 2021) and Enawo in 2017 (World Bank Group, 2017). Destructive TCs have, in some instances, been recorded in the region as far back as the late 19th century (e.g., Nash et al., 2015).

Such TCs are driven by thermodynamic and dynamic factors, including sea surface temperatures (SSTs), air temperature, relative humidity, wind shear and geopotential height (e.g., Malherbe et al., 2013; Pillay & Fitchett, 2021). Furthermore, TC genesis, intensification and track position can be affected by large-scale modes of climate variability such as the El Niño–Southern Oscillation (ENSO; Ho et al., 2006), Madden–Julian Oscillation (Bessafi & Wheeler, 2006; Duvel, 2015), Quasi-Biennial Oscillation (Jury, 1993) and Indian Ocean Subtropical Dipole and Southern Annular Mode (Matyas, 2015)—and the interplay between these conditions can also be important (Ash & Matyas, 2012). For example, the climate modelling study of Vitart et al. (2003) corroborates observations that more zonal, westward, landfalling tracks occur over Mozambique when negative ENSO conditions combine with warmer local SSTs.

A recent study using long-term reanalysis suggests a robust decrease in annual mean TC count over the 20th century for the SIO, perhaps due to a weakening of the Hadley and Walker circulations (Chand et al., 2022). However, Kossin et al. (2020) find a significant increase in the proportion of SIO TCs that are major TCs in homogenized observations during the satellite era, consistent with physical expectations given a warming tropical environment. These findings reinforce those from a previous observational study by Mavume et al. (2009).

Likewise, a recent global synthesis of several climate model projections (Knutson et al., 2020) finds that under a 2°C warming, SIO TCs decrease in frequency (albeit not with statistical significance) but significantly increase in intensity. The decrease in frequency is consistent with the projections of Malherbe et al. (2013) for the latter part of the 20th century, who used a global variable resolution climate model with its highest resolution (of approximately 60 km) focussed over the SIO. A later study with a similar modelling setup additionally projected a decrease in landfalling TCs over southern Africa (Muthige et al., 2018). More recently, the variable resolution model projection of Cattiaux et al. (2020), using 14 km as its highest focus over the SIO, found an overall 20% decrease in TC frequency accompanied by more higher-intensity TCs, for a 2°C global warming. Interestingly, complementary simulations with a uniform 50 km resolution version of their model suggested that even this resolution is potentially sufficient to generate a realistic number of TCs; however, those same lower-resolution TCs also possessed a weaker intensity. In contrast, Thompson et al. (2021) used a very high-resolution (3 km) convection-permitting regional model to project characteristics of a typical SIO TC under a pseudo global warming setup—finding an average 6.5% increase in intensity.

A significant obstacle to realistically simulating TCs is the spatial resolution of climate models, as typical grid spacings are often too coarse, and subgrid parameterisations insufficient, to adequately capture TC characteristics (e.g., Davis, 2018; Wehner et al., 2015). To assess the extent to which the most recent generation of climate models are able to capture SIO TC characteristics, this paper makes use of simulations generated by multiple high-resolution climate models that were run under the High Resolution Model Intercomparison Project (HighResMIP; Haarsma et al., 2016) of the Sixth Coupled Model Intercomparison Project (CMIP6; Eyring et al., 2016). These simulations include those from a set of models integrated at approximately 25–50 km resolution. These grid spacings have previously shown reduced biases in the simulated TC characteristics for various regions compared to lower standard resolution (typically 100 s of km) counterparts (Roberts et al., 2020a), and we will assess the biases for the SIO. Moreover, future projections with HighResMIP models have exhibited robust TC changes over the SIO, including decreases in activity (Roberts et al., 2020b), and we will assess such changes using various metrics.

For the HighResMIP simulations we consider in this study, we investigate SIO TC characteristics, including frequency, intensity, accumulated cyclone energy (ACE) and extreme wind speeds, for both a historical and future period. This is aided by using the TempestExtremes TC tracking software (Ullrich et al., 2021; Ullrich & Zarzycki, 2017). To illustrate relative biases in HighResMIP models, we compare the simulations to the European Centre for Medium-Range Weather Forecast (ECMWF) fifth European Reanalysis (ERA5; Hersbach et al., 2020).

Section 2 details the data and methods, including the reanalysis, HighResMIP simulations, and TC tracking software. Section 3 presents the results, including TC characteristics for the historical period in ERA5 and HighResMIP simulations and future changes in the latter. Sections 4 and 5 present the discussion and conclusions, respectively.

2 | DATA AND METHODS

2.1 | ERA5

ERA5 is the latest global reanalysis product from the ECMWF, combining numerical weather model data with observations from across the world into a globally complete and consistent dataset (Hersbach et al., 2020). The atmospheric component has a native grid spacing of ~31 km and is available for download on a uniform 0.25° grid at a 1-hourly frequency from 1979 to the present day, including near-surface (10-m) winds. Because of this uniform spatiotemporal coverage and consistency in the reanalysis method applied to the data over the length of the dataset, we use ERA5 as our reference dataset for achieving our aim of comparing relative biases in model TC climatology. This is as opposed to using observational products such as the International Best Track Archive for Climate Stewardship (IBTrACS; Knapp et al., 2010), where inhomogeneities over the length of the dataset can inhibit the production of an internally consistent climatology (Kuleshov et al., 2010). We accept, however, that best-guess products such as IBTrACS can provide more accurate measurements of individual TCs and that ERA5 underestimates IBTrACS observed track intensity—as found, for example, in Zarzycki et al. (2021) who note this is a common problem among reanalysis (see reference therein).

2.2 | HighResMIP simulations

We use climate model simulations from the HighResMIP, part of the CMIP6—the latest effort by the World Climate Research Programme to provide a coordinated set of climate simulations of historical and future climate from modelling centres worldwide (Eyring et al., 2016). The HighResMIP specifically provides simulations at spatiotemporal resolutions higher than the standard CMIP6 protocols. We use data from models with temporal resolutions of at least 6 h (instantaneous) and spatial resolutions of 25 km or 50 km. These resolutions have previously shown improvements in simulated TC characteristics compared to lower-resolution counterparts (Roberts et al., 2020a).

Data is available from 1950 to 2050 for many model simulations, and we only consider simulations that fully extend to 2050. Simulations have been run under the HighResMIP forcing specifications (see Roberts et al., 2020b, supplementary text S1), including the CMIP6 SSP585 high fossil fuel usage scenario (O'Neill et al., 2016) for 2015–2050, which is the scenario we consider in this study as it is expected to induce a higher climate-change-to-noise signal than lower fossil fuel usage scenarios. Data is downloaded via the Earth System Grid Federation (ESGF) portals. In cases where multiple realizations of a model's simulation are available, we select only the first realization for consistency with models with only one realization available.

We only consider models with a coupled atmosphere–ocean, as this coupling is vital to simulating more realistic features of TCs as compared to atmosphere-only simulations with prescribed sea surface temperature (e.g., Ogata et al., 2015; Scoccimarro et al., 2017; Zarzycki, 2016). Also, not all models have the requisite variables available to

TABLE 1 Outline of the HighResMIP models used.

Model name	CNRM-CM6-1-HR	CMCC-CM2-VHR4	EC-Earth3P-HR	FGOALS-f3-H	HadGEM3-GC31-HM	MPI-ESM1-2-XR
Institution	CNRM-CERFACS	CMCC	EC-Earth-Consortium	CAS	MOHC	MPI-M
Nominal resolution (resolution at 0°N)	50 km (55 km)	25 km (28 km)	50 km (39 km)	25 km (28 km)	50 km (39 km)	50 km (52 km)
All variables available for TC tracking?	Yes	No	Yes	No	No	Yes

enable TC tracking (see section 2.4). For such models, we only investigate their extreme wind speeds.

Table 1 outlines the model simulations considered. More details for these models can be found in table S1 of the supplementary material of Roberts et al. (2020b); the exception is FGOALS-f3-H, for which details can be found in Li et al. (2021).

2.3 | Analysis region and periods

For ERA5 and the HighResMIP simulations, we perform the analysis over the area used in TC forecasting by the World Meteorological Organization Regional Specialised Meteorological Center at La Reunion (e.g., Knapp et al., 2010). This area is bounded by 0°–40°S and 30°–90°E and contains much of the South Indian Ocean, Madagascar, the Mozambique Channel and southeast Africa.

We consider two 30-year periods of interest: a conventional historical period from 1980 to 2010 for both ERA5 and the HighResMIP simulations and a future period from 2020 to 2050 to investigate changes in the simulations.

2.4 | TempestExtremes TC tracking software

To track TCs in ERA5 and HighResMIP simulations, we use the TempestExtremes (TE) open-source feature tracking software (Ullrich & Zarzycki, 2017), which has been used in various TC studies to date and performs well compared to other trackers (Bourdin et al., 2022). We use version 2.2.1 of the software (very similar to that described in Ullrich et al., 2021) and the methodology outlined in Zarzycki and Ullrich (2017), which consists of a detect-and-stitch procedure for detecting tracks. First, at every 6-h time slice in the data under consideration, candidate TC nodes are located via closed-contour criteria requiring a coherent local minimum in sea-level pressure and an associated upper-level warm core characterized by decreasing thickness between geopotential surfaces. Second, candidate nodes are stitched together to form tracks according to criteria for maximum distance between nodes, minimum duration of a track (while allowing for short gaps in the track where a TC may temporarily weaken and so not meet the node location criteria), minimum magnitude and duration of near-surface wind speed, latitude, and an elevation criterion to eliminate false detections associated with thermally induced lows and sea-level pressure correction errors in regions of rough topography. Complementary to Ullrich et al. (2021), a more detailed summary of the TE algorithm used in this study can also be found in appendix B of Roberts et al. (2020a), as well as sect. 2.3 of Bourdin et al. (2022).

TE also permits the calculation of accumulated cyclone energy (ACE) for a detected TC track. ACE is a measure of TC activity and is proportional to the square of the maximum near-surface wind speed, summed over all nodes located by TE along a track (Bell et al., 2000). ACE is an increasingly popular metric for investigating TCs due to both its societal relevance and the fact that it is a more robust indicator when objective cyclone tracking algorithms are applied (Zarzycki & Ullrich, 2017).

Since TE requires at least 6-hourly sea-level pressure and atmospheric geopotential data, in addition to surface winds, this limits the models in Table 1 we can use for TC tracking. Not all models had archived these variables in the ESGF portals when this study was conducted. Specifically, we can only consider the following three models, as indicated by the bottom row of Table 1: CNRM-CM6-1-HR, EC-Earth3P-HR and MPI-ESM1-2-XR. Also, note that all three models only have a nominal resolution of 50 km (as opposed to 25 km).

2.5 | Analysis metrics

We compute the following metrics for both ERA5 and HighResMIP data for the historical period and then compute biases between the two.

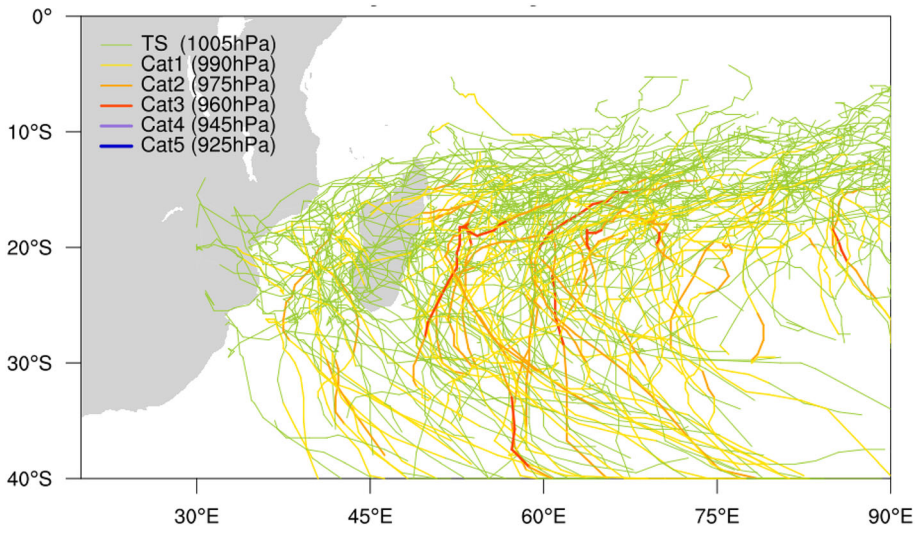

FIGURE 1 Tropical storm and cyclone tracks in ERA5 (1980–2010) from applying TE.

For the three models where TE can be applied (and for ERA5), we compute maps of all TC tracks in the analysis region over all months of the year. TC intensity along a track is categorized according to minimum sea-level pressure. We subscribe to the reasoning of Bourdin et al. (2022) in preferring to categorize according to minimum sea-level pressure rather than maximum near-surface wind speed because the former is a more reliable indicator of TCs in both models and ERA5. Furthermore, recent work also shows sea-level pressure to be better correlated to storm damage (Klotzbach et al., 2020). Following table 1 of Bourdin et al. (2022), TC categories range from 1 to 5, akin to the Saffir-Simpson scale, with pressure thresholds ranging from 990 to 925 hPa, respectively (see Figure 1); also included is a Category 0, which are tropical storms (TSs), rather than cyclones, with a pressure threshold of 1005 hPa.

From the maps of TC tracks, we also produce bar charts summarizing region-total frequency and intensity by month. For these bar charts, a track is assigned to a month according to the date at which its minimum sea-level pressure occurred (this criterion is especially required in cases where a track exists across two adjacent months). Also, for models where TE can be applied, we calculate ACE for all detected tracks in the analysis region. We furthermore compute maps of extreme (99th percentile) windspeeds over our analysis region, as these further indicate the ability of ERA5 and HighResMIP models to capture the spatial footprint of TCs. This is especially useful for those models that do not have the requisite data for TE to be applied (see section 2.4). This is done for months during the TC season for this region (October–May).

Finally, we compute all the above metrics for the future period in the model simulations, and hence the change relative to simulations for the historical period.

3 | RESULTS

3.1 | ERA5 historical climatology

The spatial pattern of tracks for the historical period in ERA5 (Figure 1) appears realistic in that TCs generally progress from the eastern South Indian Ocean toward Africa and/or poleward (e.g., Leroux et al., 2018). This pattern also agrees well with Bié and de Camargo (2023) and Ullrich et al. (2021) (see their fig. 2). However, as also shown in that later study, the density and intensity of tracks appear to underestimate best-guess observations of TS and TC tracks in IBTrACS, and we find only Category 3 tracks form at best—whereas Category 4/5 tracks form in IBTrACs data. As noted earlier, this is a common problem among reanalyses (e.g., Murakami, 2014; Schenkel & Hart, 2012; Zarzycki et al., 2021), and Cattiaux et al. (2020) report detecting an annual average of nine TCs in ERA5 compared to 13.9 for IBTrACS. We find an annual average of 4.1 TCs, but our analysis domain is smaller, our analysis period is shorter, and our tracking algorithm differs.

The distribution of the monthly count of these tracks (Figure 2) appears realistic in that the most active months are from January to March, that is, during the Southern Hemisphere summer when SSTs, a key driver of TC formation, are warmest. The distribution also agrees well with observational-based distributions in Mavume et al. (2009) and Leroux et al. (2018), albeit again with underestimation of absolute values. Also, TSs occur in more months than TCs and more frequently than individual

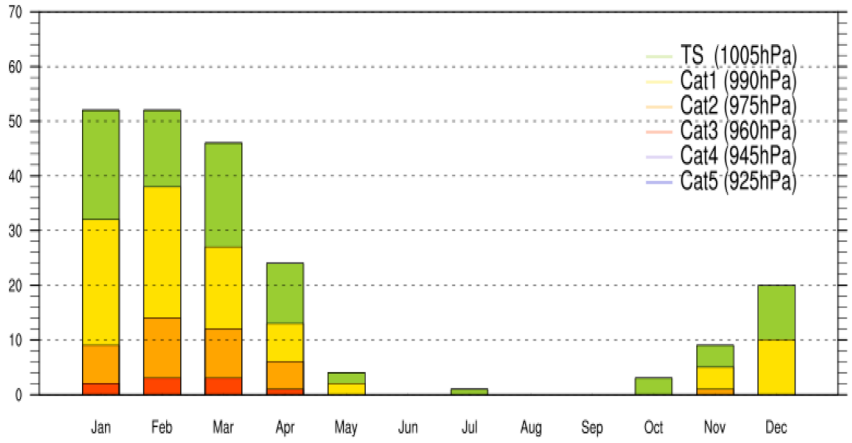

FIGURE 2 Monthly count of the tropical storm and cyclone tracks shown in Figure 1. Colours represent maximum TC intensity along a track.

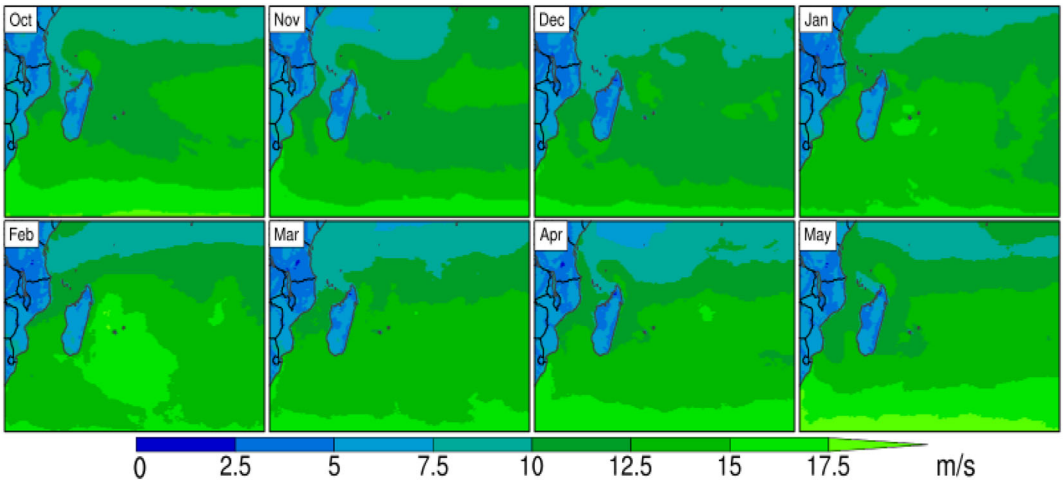

FIGURE 3 99th percentile of 10-m wind speed (1980–2010) for ERA5.

TC categories in some months—although the proportion of TCs to TSs increases in February, which is in line with SSTs being the warmest in this month.

We also examine ERA5 extreme (99th percentile) wind speed as a broad indicator of TC footprint over our analysis region (Figure 3). Winds become stronger around Madagascar in the most TC active months of January and February. Specifically, winds are stronger to the east of Madagascar, consistent with the location of higher-intensity tracks in Figure 1.

Note that we examine the 99th percentile rather than maximum wind speed because the footprint in the latter very often appears to be dominated by a single, or very few, TCs (Figure S1, Supporting Information). The same is true of the corresponding maps for the HighResMIP models (not shown). Thus, later in this study, any computation of the bias pattern between ERA5 and HighResMIP maps would be unduly dominated by a single, or very few, TCs. Hence, we prefer to examine 99th percentile wind speeds that produce a smoother footprint. We concede, however, that the strongest 99th percentile winds only reach in the region of 17.5 $m \cdot s^{-1}$ (63 kmph), which is somewhat less than required to be considered TC strength (10-min sustained winds of at least 104 kmph (28.9 $m \cdot s^{-1}$), following Bourdin et al., 2022). The maximum winds do, in some instances, appear to exceed this threshold, reaching at least 35 $m \cdot s^{-1}$ (Figure S1), which agrees with the findings of Bié and de Camargo (2023) for a similar analysis period. However, a direct comparison to sustained winds, and hence TC strengths, is not possible because ERA5 only outputs instantaneous winds.

3.2 | HighResMIP versus ERA5 historical climatology

We now examine the bias, relative to ERA5, in track frequency for the three HighResMIP models to which TE can be applied (Figure 4). Figure S2 shows the actual tracks for these models (over all categories). For the multimodel-mean (Figure 4d), models generally appear

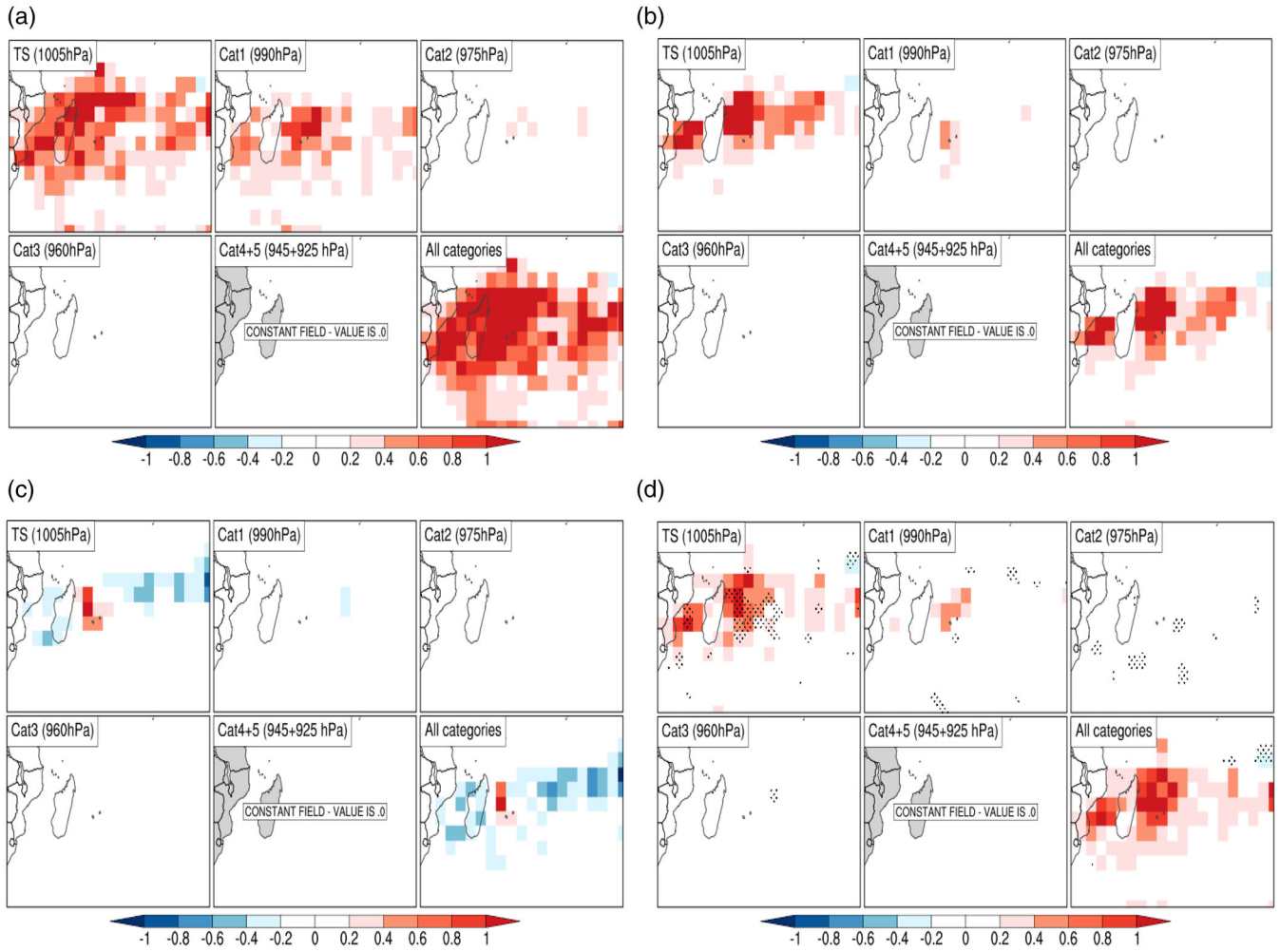

FIGURE 4 Model minus ERA5 track frequency for 1980–2010 for (a) CNRM-CM6-1-HR, (b) EC-Earth3P-HR, (c) MPI-ESM1-2-XR and (d) multimodel-mean (stippling indicates where all models agree on the sign of any difference). All data has been re-gridded to 3° resolution.

biased higher than ERA5, particularly to the east of Madagascar and in the Mozambique Channel. However, the TS signal dominates in all cases, and the individual models rarely simulate Category 3 tracks (see also Figure S2), with large variations in patterns across models.

CNRM-CM6-1-HR displays substantial biases (Figure 4a), partly due to the larger spatial extent of tracks (Figure S2a). Furthermore, Roberts et al. (2020a) note that this model uses an aerosol scheme different from all other models operating under the HighResMIP experiment design and that parameterisations related to convection may play a role in enhancing TC strength, which requires further investigation. In contrast, MPI-ESM1-2-XR is generally biased low (Figure 4c) and struggles to simulate very many tracks, with extremely few of TC strength (Figure S2c). Again, Roberts et al. (2020a, 2020b) note similar behaviour in this model, at least for Northern Hemisphere basins.

Some patterns are clear when these model biases in track frequency are broken down by month and totalled over the analysis region (Figure 5). For example, there are consistent negative biases in MPI-ESM1-2-XR, reflecting the abovementioned struggle of this model to simulate TCs. Other patterns are more mixed. For instance, although CNRM-CM6-1-HR simulates more tracks overall across the region than ERA5 in the most active months of January and February (compare Figure S3 top with Figure 2)—which is presumably what dominates the bias signal in Figure 4a—this is not the case for nearby months such as March and April, and for months at the end of the year, which display a negative bias; this later point also applies to EC-Earth3P-HR. Furthermore, CNRM-CM6-1-HR simulates an unusual amount of TCs for June, which would not be expected given cooler SSTs for that time of year. Also, there is no systematic inter-category pattern of bias across months (e.g., there is no

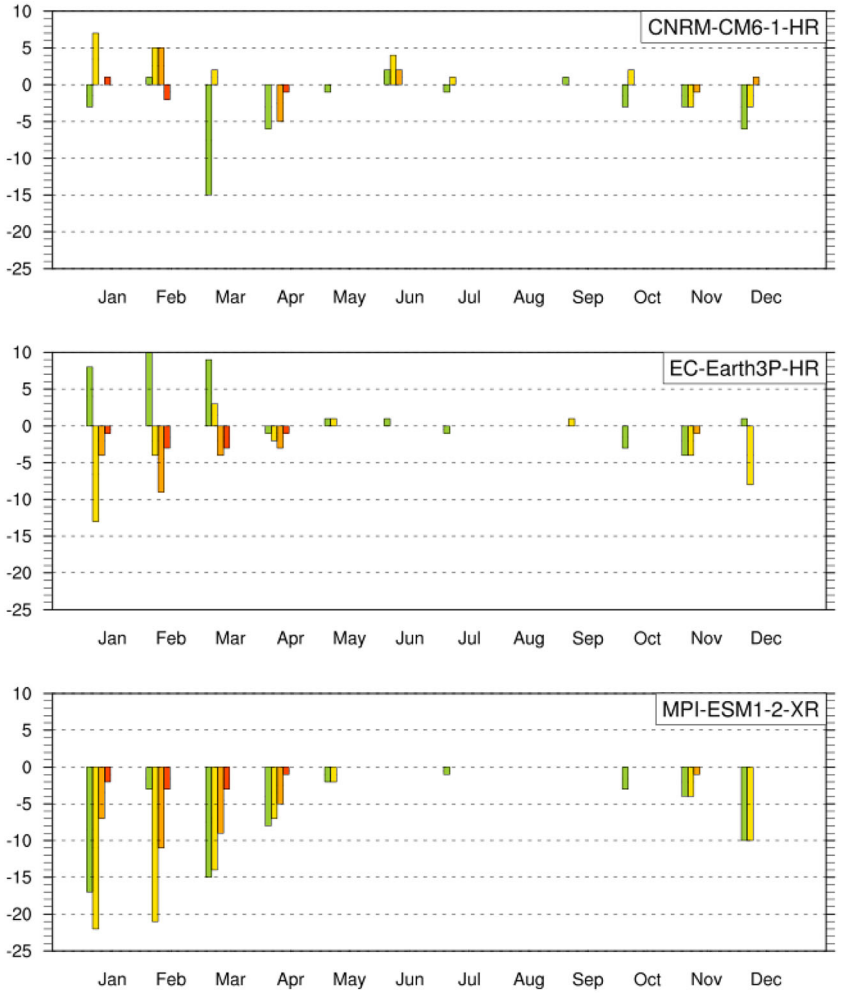

FIGURE 5 Difference, relative to ERA5, in monthly count (1980–2010) of tropical storms and cyclone tracks for (top) CNRM-CM6-1-HR, (middle) EC-Earth3P-HR and (bottom) MPI-ESM1-2-XR. Colours as in Figure 2. Note that the February TS bar for EC-Earth3P-HR has a value of 26 storms but is cut off in the plot for cosmetic reasons.

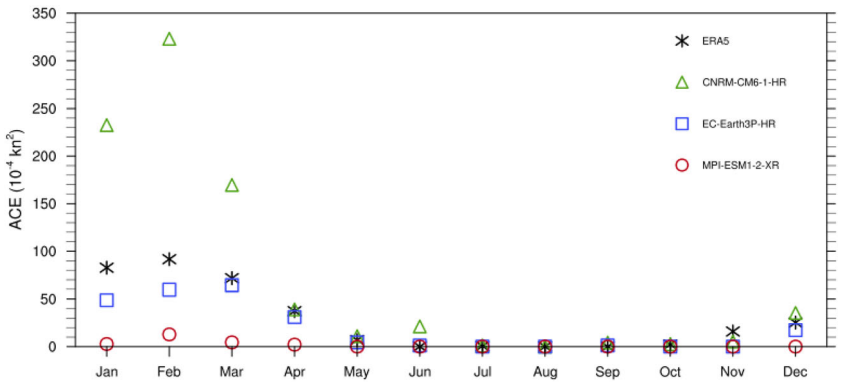

FIGURE 6 Monthly total (1980–2010) ACE over all TC tracks in ERA5 and HighResMIP models.

suggestion that Category 1 TCs are systematically more biased than Category 2 TCs across months).

Computations of ACE over the analysis region (Figure 6) exhibit features consistent with Figures 4 and 5. For example, MPI-ESM1-2-XR exhibits lower values than ERA5 for all months, and CNRM-CM6-1-HR shows higher values in January and February. The latter also exhibits higher values in March, probably reflecting that it simulated two more Category 1 TCs in that month (Figure 5, top). However, it also exhibits almost identical ACE values in April despite negative biases in Category 2 and Category 3 TC frequency—suggesting that although the model simulates fewer TCs for that month, they possess enough accumulated energy (i.e., through wind speeds and/or duration) to match that of the more numerous ERA5 TCs for that month.

We also examine the multimodel-mean bias in extreme wind speeds for all HighResMIP models (Figure 7).

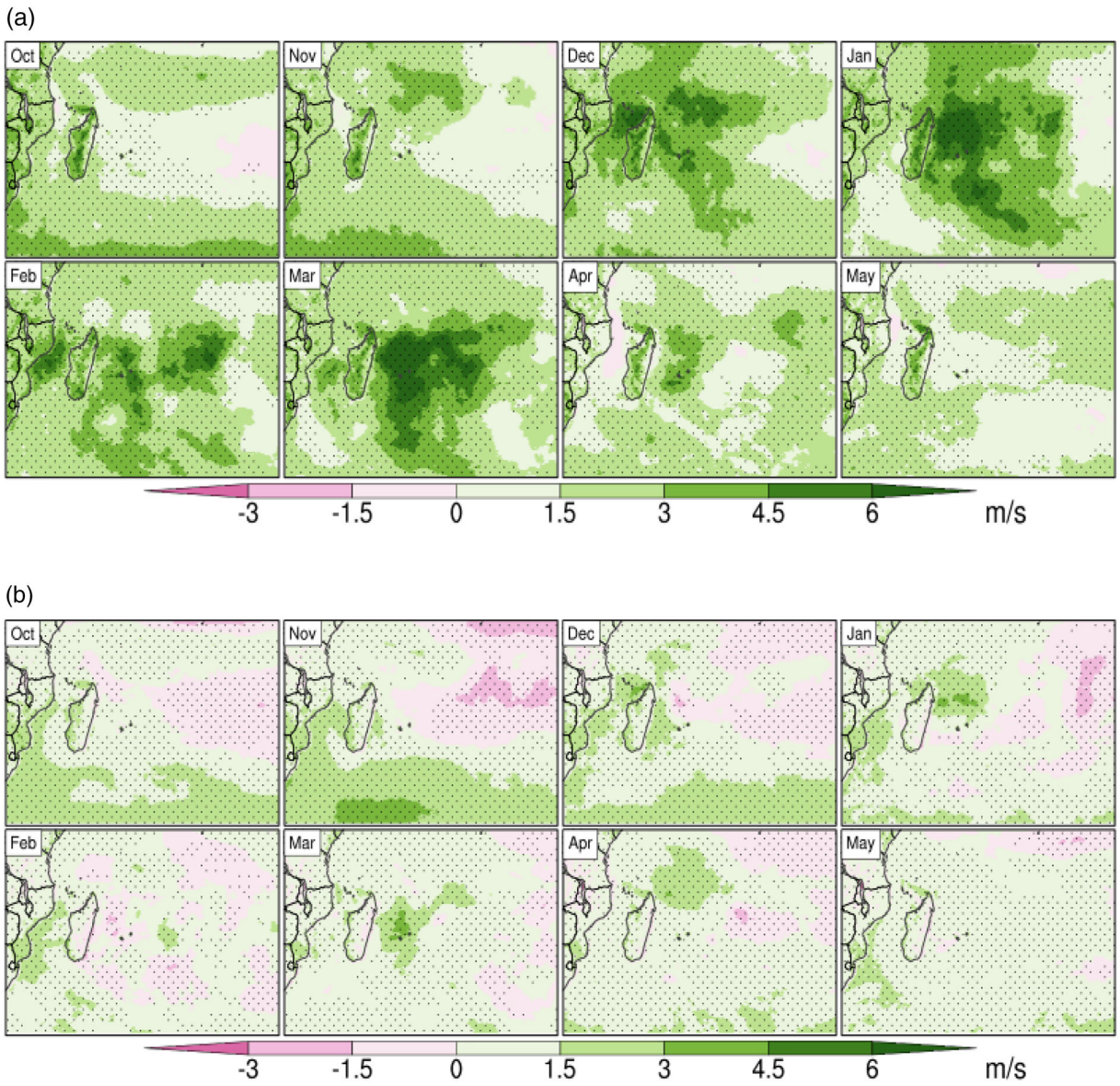

FIGURE 7 The multimodel-mean difference in 99th percentile of wind speed (1980–2010) between HighResMIP models and ERA5 for (a) 25 km nominal resolution models and (b) 50 km nominal resolution models. Stippling indicates that at least 67% of models agree with the sign of the difference.

As model resolution is an important factor in TC simulation, we separate this analysis by models with nominal 25 km and 50 km resolution (Table 1). Bias maps for individual models are shown in Figure S4.

At 25 km (Figure 7a), there are large positive biases to the east of Madagascar and somewhat in the Mozambique Channel in all active TC months. This signal is apparent in both models (Figures S4a,b) but especially in FGOALS-f3-H. Li et al. (2021) note that TC characteristics are generally enhanced in this model at this higher resolution compared to a lower resolution counterpart. Given that the spatial signature of the bias (Figure 7a) is similar to the location of tracks for models where TE tracking can be applied (Figure S2), plus that the bias is larger than that of the 50 km models (Figure 7b), this suggests that if tracking were possible for the 25 km models, we would see stronger TCs in these models than at 50 km—perhaps beyond Category 3.

At 50 km (Figure 7b), there is also limited evidence of positive biases to the east of Madagascar, in the Mozambique Channel and further south in the region. These biases appear to be dominated by CNRM-CM6-1-HR and, to some extent, by HadGEM3-GC31-HM (Figure S4c,d). This is consistent with our discussion regarding positive CNRM-CM6-1-HR biases in track frequency and ACE. We also observe that EC-Earth3P-HR

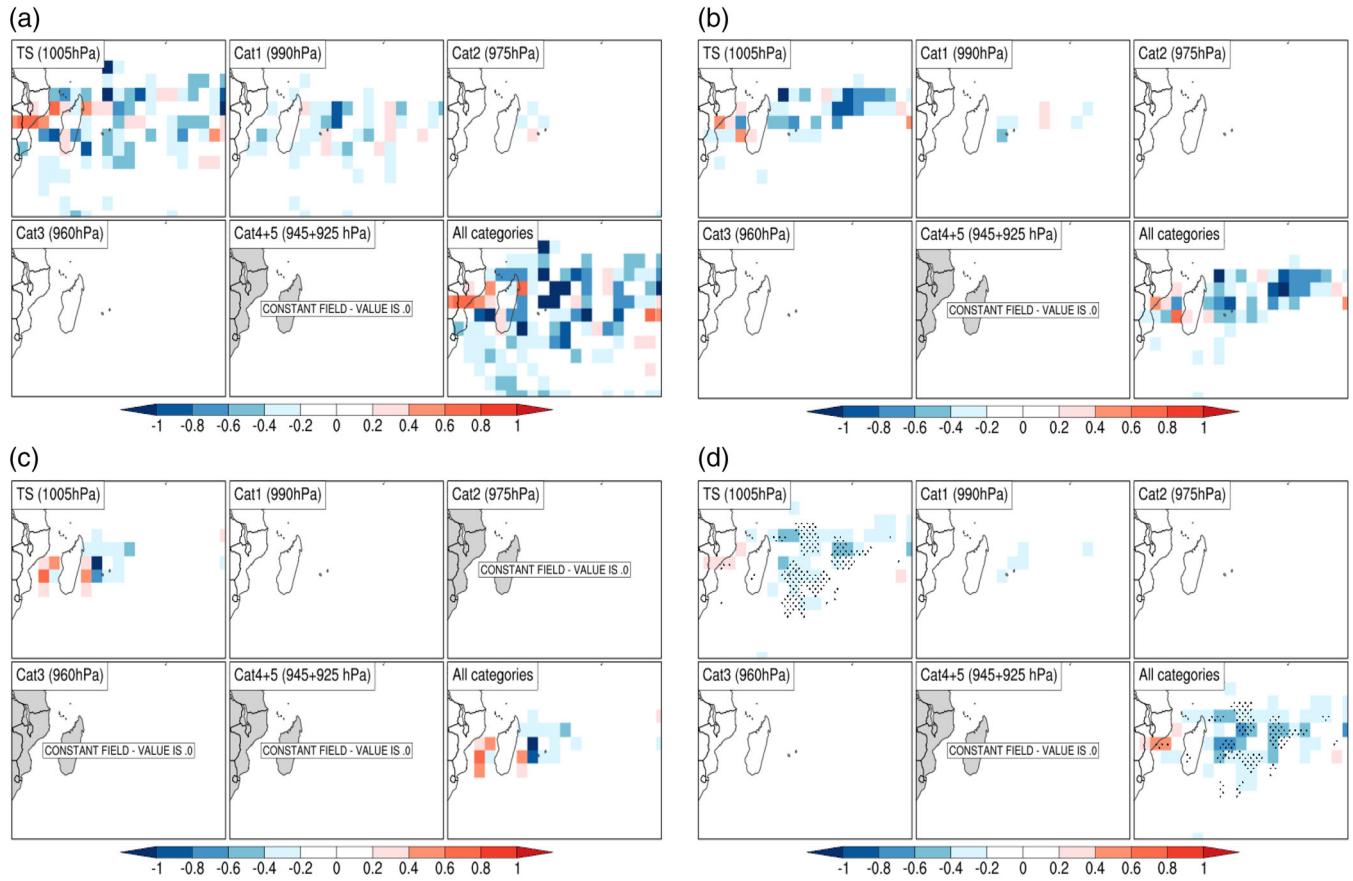

FIGURE 8 Change in tropical storm and cyclone track frequency from 1980–2010 to 2020–2050 for the (a) CNRM-CM6-1-HR, (b) EC-Earth3P-HR, (c) MPI-ESM1-2-XR, (d) multimodel-mean (stippling indicates where all models agree on the sign of any change). All data has been re-gridded to 3° resolution.

has the lowest bias (Figure S4e), perhaps because it is closest in actual resolution (39 km at 0°N) to ERA5 (31 km); this may also be why EC-Earth3P-HR ACE values, which are essentially a function of wind speed, are closest to ERA5 ACE values (Figure 6).

3.3 | HighResMIP historical versus future climatology

Changes in track frequency from the historical to the future period (Figure 8) appear mixed at the individual model level, with no appreciable changes at Category 3 and above. Mirroring the behaviour found in section 3.2, CNRM-CM6-1-HR is the most active model and MPI-ESM1-2-XR the least.

The multimodel-mean change, however, does appear more coherent, at least for the TS category—exhibiting more decreases in frequency than increases across large areas. The reductions are particularly evident to the east of Madagascar, but there are also some increases in the Mozambique Channel. This appears consistent with Roberts et al. (2020b), who found a future decrease in TC frequency over their SIO region when grouping across higher-resolution models.

When the changes in track frequency are broken down by month and totalled over the analysis region, the picture is again mixed (Figure 9). CNRM-CM6-1-HR generally shows a decrease in frequency, especially for Category 1 TCs across most months. Cattiaux et al. (2020) also find a future decrease in SIO TC frequency using a rotated-stretched atmosphere-only version of the CNRM-CM6-1. However, for higher categories, we see no systematic change across months nor any systematic intercategory relationship—albeit this may be in part due to low sample sizes. EC-Earth3P-HR also exhibits a general decrease, except notably in February. As in section 3.2, MPI-ESM1-2-XR does not produce enough tracks to allow for a meaningful analysis.

Changes in ACE for the three HighResMIP models (Figure 10) are generally negative and are consistent with the above changes in track frequency. Again, this also appears consistent with Roberts et al. (2020b), who found a future decrease in ACE over their SIO region when

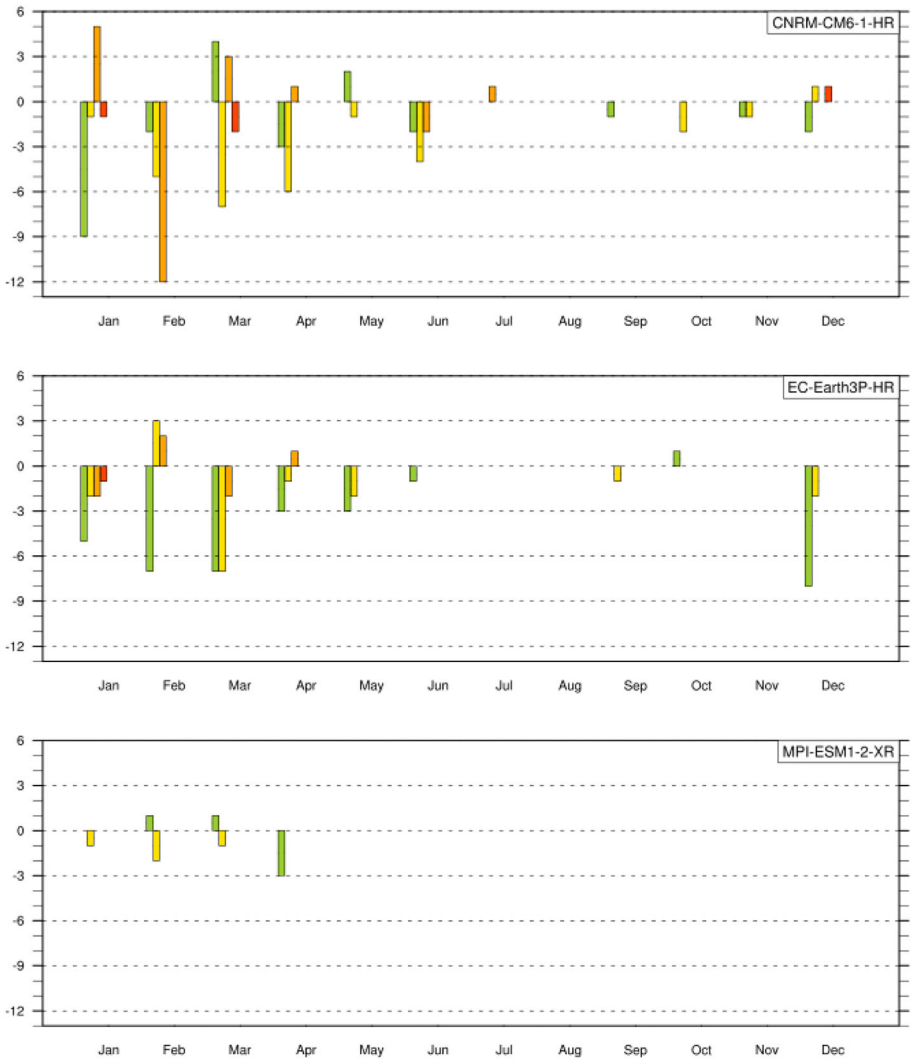

FIGURE 9 As for Figure 5, but now for the change between future and historical periods in the HighResMIP models.

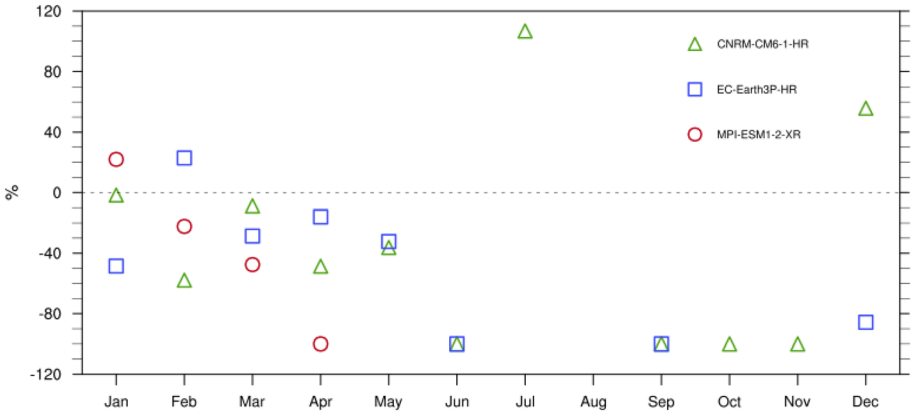

FIGURE 10 Change in monthly total (1980–2010 to 2020–2050) ACE over all TC tracks in HighResMIP models. The percentage change is undefined for months in which there were no tracks in the historical (1980–2010) period.

grouping across higher-resolution models. We find individual exceptions to the decrease for CNRM-CM6-1-HR in July due to the appearance of one additional Category 2 TC in the future period (Figure 9, top), and similarly for EC-Earth3P-HR in February due to additional Category 1 and Category 2 TCs (Figure 9, middle). For MPI-ESM1-2-XR in January, we deduce that future TSs must be strong and/or long-lived enough to increase ACE despite one fewer Category 1 TC (Figure 9, bottom).

Complementing the ACE findings, changes in multimodel-mean extreme wind speeds exhibit broad decreases (Figure 11). At 25 km resolution (Figure 11a),

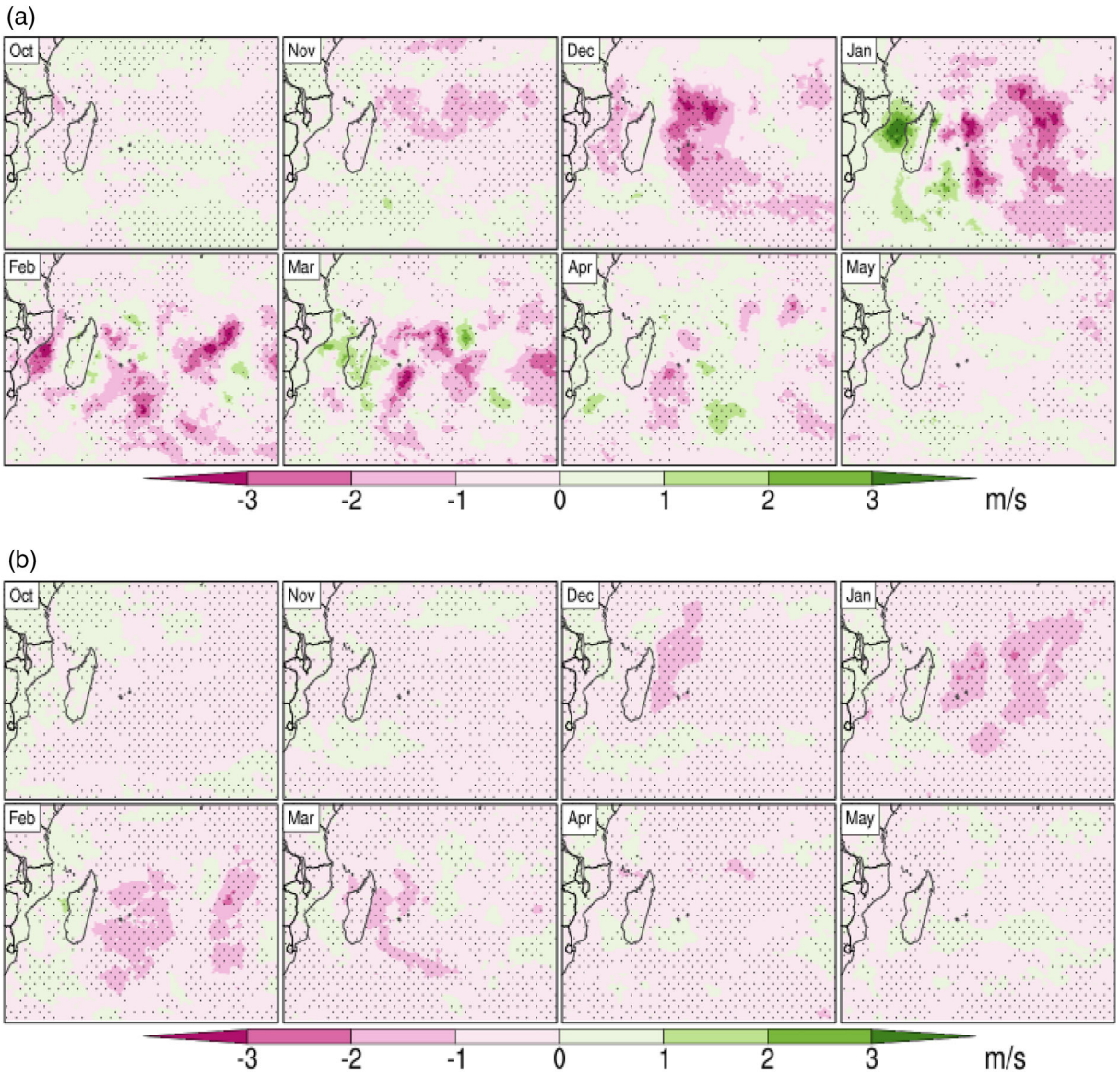

FIGURE 11 As for Figure 7, but for the change (1980–2010 to 2020–2050) in the 99th percentile of wind speed for HighResMIP models.

there is a decrease in wind speed east of Madagascar, especially from December to January, and extending somewhat into later months, with large areas of model agreement. However, agreement on strong increases in the Mozambique Channel is only apparent in January, and changes for individual models are shown in Figure S5.

The change at 50 km resolution (Figure 11b) exhibits similar but smoother characteristics to that at 25 km, reflecting the influence of the lower resolution (nevertheless, some select areas differ prominently on the sign of change compared to the 25 km resolution, e.g., in the west of the Mozambique channel in February). The change also has more extensive areas of decrease than increase overall, which seems consistent with general decreases in track frequency and ACE for the region (Figures 8d and 10).

4 | DISCUSSION

Given the relative lack of high-resolution TC climatology assessments and projections explicitly focussing on the SIO region, we took advantage of a recent set of multimodel global climate change simulations from the HighResMIP. These simulations were run at relatively high resolutions of 25–50 km, and we examined their TC characteristics over the SIO region, including computing biases against ERA5.

Both ERA5 and models produce Category 3 TCs at best (Figures 1 and S2). Reasons for this in ERA5 are likely related to insufficiently high-resolution to adequately capture TC dynamics, and deficiencies in subgrid parameterisation (Zarzycki et al., 2021). For example, Cattiaux et al. (2020) find the ERA5 pressure-wind

relationship is askew compared to IBTrACS data. Furthermore, Bié and de Camargo (2023) point out that a lack of observations for the SIO may limit the utility of data assimilation and, hence, the quality of reanalysis for this region.

Likewise, insufficient resolution and parameterisations are likely limiting the intensity of TCs in the climate models. That said, extreme wind speed biases relative to ERA5 in the 25 km models were far higher than in the 50 km models (Figure 7) and broadly in the location of the latter's TC tracks, indicating that higher than Category 3 TCs might be detected in the former, were it possible to apply tracking to them. However, Davis (2018) suggests that even models with 25 km grid spacing may still struggle with the dynamical resolution of higher category TCs—particularly a realistic wind field structure. Moreover, the results of Patricola and Wehner (2018), using a very high-resolution regional model with nonparameterised convection, suggest that grid spacings of 3 km are required to capture peak wind speeds observed in some TCs. This issue could be further explored using upcoming simulations from the next iteration of model intercomparisons (CMIP7; Dingley et al., 2023) or other very high-resolution regional modelling initiatives—though careful consideration may need to be given to the optimal positioning of the SIO domain, to simulate TC-like vortices within it (Landman et al., 2005).

Regarding model biases relative to ERA5, since the models to which TE could be applied have the same nominal resolution (50 km), this suggests that model configuration could be responsible for the considerable variation in biases (Figure 4). For example, CNRM-CM6-1-HR displays large positive biases, especially in active TC months of January and February—perhaps due to a different aerosol scheme and convective parameterisation, as discussed in Roberts et al. (2020a). Indeed, there may be a host of potential model biases at play in these results, and previous climate modelling studies have found notable TC sensitivity to model configuration, including the choice of dynamical core (e.g., Guimond et al., 2016; Reed et al., 2015), physical parameterisations (e.g., Lim et al., 2015; Reed & Jablonowski, 2011), and ocean coupling (e.g., Scoccimarro et al., 2017; Zarzycki, 2016). Further research should focus on examining the influence of these factors on the simulated TCs characteristics. One robust signal is that all models exhibit a positive bias east of Madagascar and, to a lesser extent, in the Mozambique Channel.

Similar intermodel variation in bias manifests in monthly ACE values. However, EC-Earth3P-HR ACE follows ERA5 quite closely. Additionally, it possesses the lowest model bias in near-surface wind speeds (from which ACE is derived)—perhaps reflecting the similar actual resolution between this model (∼39 km at 0°N) and ERA5 (∼31 km).

Projected changes also exhibit considerable intermodel variation (Figure 8). That said, track frequency broadly decreased across models, as did ACE (Figure 10). This is consistent with previous modelling studies that include the SIO (Knutson et al., 2020; Roberts et al., 2020b). However, like for biases in the historical period, no systematic intercategory pattern of change exists (Figure 9). Furthermore, since we can only compute changes up to a relatively limited period in the future (1980–2010 to 2020–2050), low signal-to-noise may be obscuring any such patterns. Thus, nothing meaningful can be said about relative changes between weak and strong TC intensities.

These characteristics of future changes may be better understood by exploring the underlying physical drivers, which was beyond the scope of this study but could form the basis of a follow-up study. For example, Malherbe et al. (2013) examined the physical reasons for their model-projected decreases in SIO TC occurrence, which were related to atmospheric stability, relative humidity, vertical wind shear and low-level vorticity. Muthige et al. (2018) draw similar conclusions from their model projections for up to 2°C of global warming.

The broad future decrease in extreme wind speeds east of Madagascar, accompanied by an—albeit less pronounced—increase in wind speed in the Mozambique Channel at 25 km and 50 km resolutions (Figure 11), suggests a robust east-to-west shift in track locations. This is also reflected somewhat in the multimodel-mean change in track frequency for the models to which TE could be applied (Figure 8d). Thompson et al. (2021) also find a westward, albeit small, shift in projected tracks for the case study of a typical SWIO TC. However, this may be more a consequence of their pseudo global warming experiment design.

Exploring the physical drivers behind our westward shift in track locations could again contribute to a follow-up study, and one avenue to explore could be the role of large-scale modes of climate variability. For example, it has been established that negative ENSO conditions are one component in producing more westward TC trajectories over the SIO region (Ash & Matyas, 2012; Ho et al., 2006; Vitart et al., 2003). Thus, one could investigate if such ENSO conditions are more prevalent in simulated future climates that exhibit a westward shift in TC track locations and, hence, to what extent they contribute to that shift. However, this also relies on the fidelity with which climate models can simulate ENSO.

The tendency for increases in track frequency (Figure 8) and extreme wind speed (Figure 11) to manifest in the vicinity of the Mozambique Channel is

interesting. Increased TC frequency and cyclogenesis in the channel are also suggested by Cattiaux et al. (2020) in their model projection, and the latter is in line with a greater increase in their prescribed SSTs for this area. Again, a follow-up study could investigate if local high SSTs and weak easterly vertical wind shear, which are both conducive to TC formation in this area (Matyas, 2015), are simulated to change under global warming; likewise for the role of the Mascarene high in steering TCs within this area (e.g., Ibebuchi, 2022).

5 | CONCLUSIONS

We have assessed the characteristics of SIO TCs using high-resolution (nominally 25–50 km) coupled atmosphere–ocean climate model simulations from the HighResMIP. This assessment firstly comprised a quantification of historical period TCs in ERA5 and model biases relative to ERA5, and secondly, a quantification of future changes in the model compared to the historical period. To facilitate the assessment, we applied TE software to track TCs. Data availability limited the application of TE to only three of the six available HighResMIP models (and those three coincidentally only had 50 km nominal resolution). Thus, we also resorted to examining extreme near-surface wind speeds in all six models as a proxy for TC footprints. We also quantified lower-intensity TSs alongside the TCs.

For the historical period, ERA5 exhibits realistic spatial patterns of TS and TC tracks and a realistic monthly distribution. However, it underestimates intensities, with detected TCs only reaching Category 3 on the Saffir-Simpson scale. HighResMIP model track frequencies and ACE show mixed biases relative to ERA5, with considerable intermodel variation and again Category 3 TCs at best. This variation is likely due to differences in individual model configurations that require further investigation. However, one robust bias signal across models is a positive bias east of Madagascar and, to a lesser extent, in the Mozambique Channel. No systematic intercategory pattern of bias exists across months (e.g., Category 1 TCs are not systematically more biased than Category 2).

A considerable intermodel spread was also present in the future changes. Mirroring the historical period, CNRM-CM6-1-HR remained the most active model and MPI-ESM1-2-XR the least across all relevant analysis metrics. Nevertheless, track frequency broadly decreased across models for the region, as did ACE. With respect to changes in individual TC categories, however, no systematic intercategory pattern of change emerges (e.g., Category 2 TCs do not systematically increase more than Category 1). Thus, we cannot conclude anything meaningful regarding potential changes in more intense TCs relative to less intense ones.

Across models, a broad future east-to-west shift in track locations, from east of Madagascar into the vicinity of the Mozambique channel, is indicated. Changes in extreme wind speed at both 25 km and 50 km—particularly featuring decreases in wind speeds east of Madagascar—also suggest this shift. Identifying the reasons behind such a shift is beyond the scope of this paper. This would require a deeper investigation of the physical drivers of SIO TCs, including the role of thermodynamic and dynamic factors and large-scale modes of climate variability.

Our study, which finds models capable of simulating Category 3 TCs at best and uses extreme wind speeds as a proxy for TC footprints, can point to some historical characteristics of SIO TCs and potential future changes. However, further high-resolution modelling initiatives would be welcome to deepen the analysis of this lesser-modelled region. Pillay and Fitchett (2021) also note the underrepresentation of the Southern Hemisphere in the literature regarding TC drivers and climatology. Efforts such as the interdisciplinary ReNovRisk programme (Tulet et al., 2021) have sought to investigate SIO region TCs hazards and their physical and socio-economic impacts. Additionally, such modelling efforts may inform initiatives like the RC3 project (RC3, 2021), which aimed to improve resilience to TCs in this particularly vulnerable part of the world.

AUTHOR CONTRIBUTIONS

Pardeep Pall: Writing – original draft; investigation; visualization; methodology; software; formal analysis; writing – review and editing. **Alexandre S. Gagnon:** Conceptualization; investigation; writing – review and editing; supervision; methodology. **Massimo A. Bollasina:** Conceptualization; investigation; writing – review and editing; supervision; methodology. **Colin M. Zarzycki:** Software; writing – review and editing; methodology. **Yuner Huang:** Funding acquisition; conceptualization; writing – review and editing. **Christopher T. S. Beckett:** Conceptualization; funding acquisition; writing – review and editing. **Harinaivo Ramanantoanina:** Funding acquisition; resources; project administration. **Thomas P. S. Reynolds:** Funding acquisition; conceptualization; project administration; writing – review and editing.

ACKNOWLEDGEMENTS

We thank all the members of the RC3 project for their insights and guidance and an anonymous reviewer for their very helpful suggestions. The work presented in this paper was funded through the Royal Society Challenge Grant CHL\R1\180180.

CONFLICT OF INTEREST STATEMENT

The authors declare no conflicts of interest.

DATA AVAILABILITY STATEMENT

HighResMIP data is available through the federated ESGF nodes (https://esgf.llnl.gov). ERA5 data is available through the Copernicus Climate Change Service Climate Data Store (https://cds.climate.copernicus.eu). Version 2.2.1 of TempestExtremes is available via ZENODO (https://zenodo.org/records/5908354).

ORCID

Pardeep Pall https://orcid.org/0000-0002-2380-0874

REFERENCES

AON. (2022) Global catastrophe recap first half of 2022. Available from: https://www.aon.com/reinsurance/thoughtleadership/default/global-catastrophe-recap-1h-2022 [Accessed on 11th June 2023]

Ash, K.D. & Matyas, C.J. (2012) The influences of ENSO and the subtropical Indian Ocean Dipole on tropical cyclone trajectories in the South Indian Ocean. *International Journal of Climatology*, 32, 41–56. Available from: https://doi.org/10.1002/joc.2249

Bell, G.D., Halpert, M.S., Schnell, R.C., Higgins, R.W., Lawrimore, J., Kousky, V.E. et al. (2000) Climate assessment for 1999. *Bulletin of the American Meteorological Society*, 81(6), S1–S50. Available from: https://doi.org/10.1175/1520-0477(2000)81[s1:CAF]2.0.CO;2

Bessafi, M. & Wheeler, M.C. (2006) Modulation of South Indian Ocean tropical cyclones by the Madden–Julian Oscillation and convectively coupled equatorial waves. *Monthly Weather Review*, 134, 638–656.

Bié, A.J. & de Camargo, R. (2023) Tropical cyclones position and intensity in the Southwest Indian Ocean as represented by CFS and ERA5 atmospheric reanalysis datasets. *International Journal of Climatology*, 43(10), 4532–4551. Available from: https://doi.org/10.1002/joc.8101

Bourdin, S., Fromang, S., Dulac, W., Cattiaux, J., & Chauvin, F. (2022) Intercomparison of four algorithms for detecting tropical cyclones using ERA5. *Geoscientific Model Development*, 15(17), 6759–6786. Available from: https://doi.org/10.5194/gmd-15-6759-2022

Cattiaux, J., Chauvin, F., Bousquet, O., Malardel, S. & Tsai, C.L. (2020) Projected changes in the Southern Indian Ocean cyclone activity assessed from high-resolution experiments and CMIP5 models. *Journal of Climate*, 33(12), 4975–4991. Available from: https://doi.org/10.1175/JCLI-D-19-0591.1

Chand, S.S., Walsh, K.J.E., Camargo, S.J., Kossin, J.P., Tory, K.J., Wehner, M.F. et al. (2022) Declining tropical cyclone frequency under global warming. *Nature Climate Change*, 12, 655–661. Available from: https://doi.org/10.1038/s41558-022-01388-4

Chang-Seng, D.S. & Jury, M.R. (2010) Tropical cyclones in the SW Indian Ocean. Part 2: structure and impacts at the event scale. *Meteorology and Atmospheric Physics*, 106, 163–178. Available from: https://doi.org/10.1007/s00703-010-0059-y

Davis, C.A. (2018) Resolving tropical cyclone intensity in models. *Geophysical Research Letters*, 45, 2082–2087. Available from: https://doi.org/10.1002/2017GL076966

Dingley, B., O'Rourke, E. & Turner, B. (2023) CMIP panel members, WGCM infrastructure panel members, and CMIP7 task team members, 2023: CMIP annual report 2022–2023. https://doi.org/10.5281/zenodo.8101810

Duvel, J.P. (2015) Initiation and intensification of tropical depressions over the southern Indian Ocean: influence of the MJO. *Monthly Weather Review*, 143(6), 2170–2191. Available from: https://doi.org/10.1175/MWR-D-14-00318.1

Eyring, V., Bony, S., Meehl, G.A., Senior, C.A., Stevens, B., Stouffer, R.J. et al. (2016) Overview of the Coupled Model Intercomparison Project Phase 6 (CMIP6) experimental design and organization. *Geoscientific Model Development*, 9, 1937–1958. Available from: https://doi.org/10.5194/gmd-9-1937-2016

Fitchett, J. (2018) Recent emergence of CAT5 tropical cyclones in the South Indian Ocean. *South African Journal of Science*, 114(11/12), 4426. Available from: https://doi.org/10.17159/sajs.2018/4426

Guimond, S.R., Reisner, J.M., Marras, S. & Giraldo, F.X. (2016) The impacts of dry dynamic cores on asymmetric hurricane intensification. *Journal of the Atmospheric Sciences*, 73(12), 4661–4684. Available from: https://doi.org/10.1175/JAS-D-16-0055.1

Haarsma, R.J., Roberts, M.J., Vidale, P.L., Senior, C.A., Bellucci, A. & Bao, Q. (2016) High Resolution Model Intercomparison Project (HighResMIP v1.0) for CMIP6. *Geoscientific Model Development*, 9, 4185–4208. Available from: https://doi.org/10.5194/gmd-9-4185-2016

Hersbach, H., Bell, B., Berrisford, P., Hirahara, S., Horányi, A. & Muñoz-Sabater, J. (2020) The ERA5 global reanalysis. *Quarterly Journal of the Royal Meteorological Society*, 146(730), 1999–2049.

Ho, C., Kim, J., Jeong, J., Kim, H. & Chen, D. (2006) Variation of tropical cyclone activity in the South Indian Ocean: El Nino Southern Oscillation and Madden–Julian Oscillation effects. *Journal of Geophysical Research: Atmospheres*, 111, D22101. Available from: https://doi.org/10.1029/2006JD007289

Ibebuchi, C.C. (2022) Can synoptic patterns influence the track and formation of tropical cyclones in the Mozambique Channel? *AIMS Geosciences*, 8(1), 33–51. Available from: https://doi.org/10.3934/geosci.2022003

JBA Risk Management. (2023) Tropical cyclone Freddy: February–March 2023. Available from: https://www.jbarisk.com/products-services/event-response/tropical-cyclone-freddy-february-march-2023/ [Accessed on 11th June 2023]

Jury, M.R. (1993) A preliminary study of climatological associations and characteristics of tropical cyclones in the SW Indian Ocean. *Meteorology and Atmospheric Physics*, 51, 101–115.

Klotzbach, P.J., Bell, M.M., Bowen, S.G., Gibney, E.J., Knapp, K.R. & Schreck, C.J. (2020) Surface pressure a more skillful predictor of normalized hurricane damage than maximum sustained wind. *Bulletin of the American Meteorological Society*, 101, E830–E846. Available from: https://doi.org/10.1175/BAMS-D-19-0062.1

Knapp, K.R., Kruk, M.C., Levinson, D.H., Diamond, H.J. & Neumann, C.J. (2010) The International Best Track Archive for Climate Stewardship (IBTrACS): unifying tropical cyclone best track data. *Bulletin of the American Meteorological Society*, 91, 363–376. Available from: https://doi.org/10.1175/2009BAMS2755.1

Knutson, T.R., Camargo, S.J., Chan, J.C.L., Emanuel, K., Ho, C.-H., Kossin, J. et al. (2020) Tropical cyclones and climate change

assessment: part II. Projected response to anthropogenic warming. *Bulletin of the American Meteorological Society*, 101, E303–E322. Available from: https://doi.org/10.1175/bams-d-18-0194.1

Kossin, J.P., Knapp, K.R., Olander, T.L. & Velden, C.S. (2020) Global increase in major tropical cyclone exceedance probability over the past four decades. *Proceedings of the National Academy of Sciences of the United States of America*, 117(22), 11975–11980. Available from: https://doi.org/10.1073/pnas.1920849117

Kuleshov, Y., Fawcett, R., Qi, L., Trewin, B., Jones, D., McBride, J. et al. (2010) Trends in tropical cyclones in the South Indian Ocean and the South Pacific Ocean. *Journal of Geophysical Research: Atmospheres*, 115(1), 1–9. Available from: https://doi.org/10.1029/2009JD012372

Landman, W.A., Seth, A. & Camargo, S.J. (2005) The effect of regional climate model domain choice on the simulation of tropical cyclone-like vortices in the southwestern Indian Ocean. *Journal of Climate*, 18, 1263–1274.

Leroux, M.D., Meister, J., Mekies, D. & Dorla, A.L. (2018) A climatology of Southwest Indian Ocean tropical systems: their number, tracks, impacts, sizes, empirical maximum potential intensity, and intensity changes. *Journal of Applied Meteorology and Climatology*, 57, 1021–1041. Available from: https://doi.org/10.1175/JAMC-D-17-0094.1

Li, J., Bao, Q., Liu, Y., Wang, L., Yang, J., Wu, G. et al. (2021) Effect of horizontal resolution on the simulation of tropical cyclones in the Chinese Academy of Sciences FGOALS-f3 climate system model. *Geoscientific Model Development*, 14, 6113–6133. Available from: https://doi.org/10.5194/gmd-14-6113-2021

Lim, Y.-K., Schubert, S.D., Reale, O., Lee, M.-I., Molod, A.M. & Suarez, M.J. (2015) Sensitivity of tropical cyclones to parameterized convection in the NASA GEOS-5 model. *Journal of Climate*, 28(2), 551–573. Available from: https://doi.org/10.1175/JCLI-D-14-00104.1

Malherbe, J., Engelbrecht, F.A. & Landman, W.A. (2013) Projected changes in tropical cyclone climatology and landfall in the Southwest Indian Ocean region under enhanced anthropogenic forcing. *Climate Dynamics*, 40(11–12), 2867–2886. Available from: https://doi.org/10.1007/s00382-012-1635-2

Matyas, C.J. (2015) Tropical cyclone formation and motion in the Mozambique Channel. *International Journal of Climatology*, 3, 375–390. Available from: https://doi.org/10.1002/joc.3985

Mavume, A., Rydberg, L., Rouault, M. & Lutjeharms, J. (2009) Climatology and landfall of tropical cyclones in the South-West Indian Ocean. *Western Indian Ocean Journal of Marine Science*, 8(1), 19–39. Available from: https://doi.org/10.4314/wiojms.v8i1.56672

Murakami, H. (2014) Tropical cyclones in reanalysis data sets. *Geophysical Research Letters*, 41, 2133–2141. Available from: https://doi.org/10.1002/2014GL059519

Muthige, M.S., Malherbe, J., Englebrecht, F.A., Grab, S., Beraki, A., Maisha, T.R. et al. (2018) Projected changes in tropical cyclones over the Southwest Indian Ocean under different extents of global warming. *Environmental Research Letters*, 13(6), 065019.

Nash, D.J., Pribyl, K., Klein, J., Endfield, G.H., Kniveton, D.R. & Adamson, G.C. (2015) Tropical cyclone activity over Madagascar during the late nineteenth century. *International Journal of Climatology*, 35(11), 3249–3261. Available from: https://doi.org/10.1002/joc.4204

Nhundu, K., Sibanda, M. & Chaminuka, P. (2021) Economic losses from cyclones Idai and Kenneth and Floods in southern Africa: implications on sustainable development goals. In: Nhamo, G. & Chikodzi, D. (Eds.) *Cyclones in southern Africa. Sustainable development goals series*. Cham: Springer. Available from: https://doi.org/10.1007/978-3-030-74303-1_19

O'Neill, B.C., Tebaldi, C., van Vuuren, D.P., Eyring, V., Friedlingstein, P., Hurtt, G. et al. (2016) The Scenario Model Intercomparison Project (ScenarioMIP) for CMIP6. *Geoscientific Model Development*, 9(9), 3461–3482. Available from: https://doi.org/10.5194/gmd-9-3461-2016

Ogata, T., Mizuta, R., Adachi, Y., Murakami, H. & Ose, T. (2015) Effect of air–sea coupling on the frequency distribution of intense tropical cyclones over the northwestern Pacific. *Geophysical Research Letters*, 42(23), 10415–10421. Available from: https://doi.org/10.1002/2015gl066774

Patricola, C.M. & Wehner, M.F. (2018) Anthropogenic influences on major tropical cyclone events. *Nature*, 563(7731), 339–346. Available from: https://doi.org/10.1038/s41586-018-0673-2

Pillay, M.T. & Fitchett, J.M. (2021) On the conditions of formation of Southern Hemisphere tropical cyclones. *Weather and Climate Extremes*, 34, 100376. Available from: https://doi.org/10.1016/j.wace.2021.100376

RC3. (2021) Resilience of traditional structures in Madagascar to cyclones in a changing climate (RC3). Available from: https://blogs.ed.ac.uk/rc3project/ [Accessed on 24th August 2023]

Reed, K.A. & Jablonowski, C. (2011) Impact of physical parameterizations on idealized tropical cyclones in the Community Atmosphere Model. *Geophysical Research Letters*, 38(4), L04805. Available from: https://doi.org/10.1029/2010GL046297

Reed, K.A., Bacmeister, J.T., Rosenbloom, N.A., Wehner, M.F., Bates, S.C., Lauritzen, P.H. et al. (2015) Impact of the dynamical core on the direct simulation of tropical cyclones in a high-resolution global model. *Geophysical Research Letters*, 42(9), 3603–3608. Available from: https://doi.org/10.1002/2015GL063974

Roberts, M.J., Camp, J., Seddon, J., Vidale, P.L., Hodges, K., Vanniere, B. et al. (2020a) Impact of model resolution on tropical cyclone simulation using the HighResMIP–PRIMAVERA multimodel ensemble. *Journal of Climate*, 33(7), 2557–2583. Available from: https://doi.org/10.1175/JCLI-D-19-0639.1

Roberts, M.J., Camp, J., Seddon, J., Vidale, P.L., Hodges, K., Vannière, B. et al. (2020b) Projected future changes in tropical cyclones using the CMIP6 HighResMIP multimodel ensemble. *Geophysical Research Letters*, 47, e2020GL088662. Available from: https://doi.org/10.1029/2020GL088662

Schenkel, B.A. & Hart, R.E. (2012) An examination of tropical cyclone position, intensity, and intensity life cycle within atmospheric reanalysis datasets. *Journal of Climate*, 25, 3453–3475. Available from: https://doi.org/10.1175/2011JCLI4208.1

Scoccimarro, E., Fogli, P.G., Reed, K.A., Gualdi, S., Masina, S. & Navarra, A. (2017) Tropical cyclone interaction with the ocean: the role of high-frequency (subdaily) coupled processes. *Journal of Climate*, 30(1), 145–162. Available from: https://doi.org/10.1175/jcli-d-16-0292.1

Seneviratne, S.I., Zhang, X., Adnan, M., Badi, W., Dereczynski, C., Di Luca, A. et al. (2021) Weather and climate extreme events in a changing climate. In: Masson-Delmotte, V., Zhai, P., Pirani, A., Connors, S.L., Péan, C., Berger, S. et al. (Eds.)

Climate change 2021: the physical science basis. Contribution of working group I to the sixth assessment report of the Intergovernmental Panel on Climate Change. Cambridge and New York, NY: Cambridge University Press, pp. 1513–1766. Available from: https://doi.org/10.1017/9781009157896.013

Thompson, C., Barthe, C., Bielli, S., Tulet, P. & Pianezze, J. (2021) Projected characteristic changes of a typical tropical cyclone under climate change in the Southwest Indian Ocean. *Atmosphere*, 12, 232. Available from: https://doi.org/10.3390/atmos12020232

Tulet, P., Aunay, B., Barruol, G., Barthe, C., Belon, R., Bielli, S. et al. (2021) ReNovRisk: a multidisciplinary programme to study the cyclonic risks in the South-West Indian Ocean. *Natural Hazards*, 107, 1191–1223. Available from: https://doi.org/10.1007/s11069-021-04624-w

Ullrich, P.A. & Zarzycki, C.M. (2017) TempestExtremes: a framework for scale-insensitive pointwise feature tracking on unstructured grids. *Geoscientific Model Development*, 10, 1069–1090. Available from: https://doi.org/10.5194/gmd-10-1069-2017

Ullrich, P.A., Zarzycki, C.M., McClenny, E.E., Pinheiro, M.C., Stansfield, A.M. & Reed, K.A. (2021) TempestExtremes v2.1: a community framework for feature detection, tracking, and analysis in large datasets. *Geoscientific Model Development*, 14, 5023–5048. Available from: https://doi.org/10.5194/gmd-14-5023-2021

Vitart, F., Anderson, D. & Stockdale, T. (2003) Seasonal forecasting of tropical cyclone landfall over Mozambique. *Journal of Climate*, 16, 3932–3945.

Wehner, M., Reed, K.A., Stone, D., Collins, W.D. & Bacmeister, J. (2015) Resolution dependence of future tropical cyclone projections of CAM5.1 in the U.S. CLIVAR Hurricane Working Group idealized configurations. *Journal of Climate*, 28, 3905–3925. Available from: https://doi.org/10.1175/JCLI-D-14-00311.1

World Bank Group. (2017) Estimation of economic losses from tropical cyclone Enawo. Available from: https://reliefweb.int/attachments/545f36e8-7658-35f6-8fa7-f80953abc54a/MG-Report-on-the-Estimation-of-Economic-Losses.pdf [Accessed on 11th June 2023]

Zarzycki, C.M. & Ullrich, P.A. (2017) Assessing sensitivities in algorithmic detection of tropical cyclones in climate data. *Geophysical Research Letters*, 44, 1141–1149. Available from: https://doi.org/10.1002/2016GL071606

Zarzycki, C.M. (2016) Tropical cyclone intensity errors associated with lack of two-way ocean coupling in high-resolution global simulations. *Journal of Climate*, 29(23), 8589–8610. Available from: https://doi.org/10.1175/jcli-d-16-0273.1

Zarzycki, C.M., Ullrich, P.A. & Reed, K.A. (2021) Metrics for evaluating tropical cyclones in climate data. *Journal of Applied Meteorology and Climatology*, 60, 643–660.

SUPPORTING INFORMATION

Additional supporting information can be found online in the Supporting Information section at the end of this article.

How to cite this article: Pall, P., Gagnon, A. S., Bollasina, M. A., Zarzycki, C. M., Huang, Y., Beckett, C. T. S., Ramanantoanina, H., & Reynolds, T. P. S. (2024). Assessing South Indian Ocean tropical cyclone characteristics in HighResMIP simulations. *International Journal of Climatology*, 1–17. https://doi.org/10.1002/joc.8609